



Major reshaping of narrow beams by resonant multilayer structures

V. B. YURCHENKO,^{1,*} M. CIYDEM,¹ M. L. GRADZIEL,² AND J. A. MURPHY²

¹*Engitek Engineering Technologies Ltd, 197/16 Ceyhan Atif Kansu, 06460, Ankara, Turkey*

²*Maynooth University Department of Experimental Physics, Maynooth, Ireland*

*v.yurchenko.nuim@gmail.com

Abstract: Major reshaping of electromagnetic MM-wave beams transmitted at resonant frequencies through high-quality multilayer structures is demonstrated. Beam reshaping emerges due to efficient excitation of intrinsic quasi-optical modes with complex spatial profiles by an incident beam. This leads to a significant increase of width and distortion of shape of transmitted beams, which grow with increasing likelihood of excitation of higher-order modes. The beam shape is extremely sensitive to imperfections of real structures and can become complex and asymmetric even at the normal-angle transmission of symmetric incident beams. The effect is of importance for the resonant MM-wave and THz spectroscopy of low-loss dielectric materials.

© 2020 Optical Society of America under the terms of the [OSA Open Access Publishing Agreement](#)

1. Introduction

We investigate major reshaping of electromagnetic wave beams by planar multilayer structures with high values of quality factor Q at the resonant transmission frequencies. The effect appears due to excitation of high-amplitude intrinsic quasi-optical modes with complex spatial profiles by an incident beam. This leads to a significant increase of beam width behind the resonant structure and distortion of transmitted beam. The beam profile is extremely sensitive to irregularities of real structures and can become complex even at the normal transmission of symmetric incident beam. We consider conventional uniform isotropic materials with planar and parallel interfaces between the layers, which exclude any chiral, anisotropic, and beam-focusing properties of multilayer structures. No active or nonlinear media are involved so that reshaping of beams occurs through perfectly linear wave propagation process.

Interaction of waves with material layers, interfaces, and multilayer structures is a canonical area of research producing a huge body of work on a variety of topics [1]. Transmission and reflection of beams at a single interface or a dielectric layer is a key topic [2–4] that concerns any kinds of waves and frequency bands [5–8]. The material interfaces alter the shape, position, and polarization state of transmitted and reflected beams due to variability of transmission and reflection coefficients of partial plane waves constituting the beams. Reshaping of beams is usually small [2,6] whereas the change in position is more noticeable, especially, at the oblique incidence in the range of angles of total reflection [3–8].

In general, the beams are slightly shifted in longitudinal and transverse directions along the interface with respect to geometrical optics predictions. The shifts are known as the Goos-Hänchen (GH) and Imbert-Fedorov (IF) spatial effects, respectively, which have their angular counterparts, i.e., deflections of beams due to the relevant shifts in the momentum space [9–11]. The effects are the most noticeable at the angles of total reflection. Consequently, research efforts are very much confined to the study of these effects at the oblique beam incidence.

The main body of research is focused on developing techniques for enhancing nonspecular effects, which involve the use of multilayer structures [12–14], nonconventional materials (graphene) [15,16], plasmonic resonances [17,18], surface Bloch waves [19], linear and nonlinear

photonic crystals (PCs) [20–22], bianisotropic (left-handed) metamaterials [23,24], nonlinear media with electromagnetically induced transparency [25,26], and other approaches.

The issue close to our interests is the enhancement of nonspecular effects at the oblique incidence on multilayer structures [12–14]. In a single layer, the effects are small because all the constituent plane waves are transformed in a comparable manner and remain of nearly the same proportions in both the reflected and transmitted beams [2,6]. Multilayered media produce greater effects since their reflectance function can vary more rapidly [13,14]. As a result, significant reshaping of beams would also occur.

A much greater reshaping of beams should appear due to another phenomenon, which is a resonant increase of the wave field in an high- Q resonator. For scalar Gaussian beams at oblique incidence, a prediction exists that a great lateral shift and expansion of reflected and transmitted beams should occur in a model PC with a defect layer [27]. A giant shift of reflected beams, also at oblique incidence, is predicted for another PC where graphene film is embedded in a defect layer for producing variable conductivity at the resonant frequency in the infrared band [28].

In distinction from the cited research, we carry out experiments and simulations, which demonstrate major expansion, non-uniform reshaping, and irregular distortions of narrow millimeter-wave (MM-wave) beams transmitted through highly-resonant structures at normal incidence. The effect is crucial for various applications, e.g., for THz and MM-wave dielectric spectroscopy of materials [29–32], light-controlled MM-wave beam switches [33], etc.

We investigate the expansion of beams by Bragg assemblies composed of electrically-fused quartz wafers with resonant layer insertions, which function as quasi-optical resonators in the MM-wave band. The assemblies provide a resonant transmission with $Q \approx 10^3$ at the peak frequencies $f_p = 90 - 100$ GHz observed in the propagation bandgap $f = 75 - 110$ GHz, which is the measurement band of the Vector Network Analyzer (VNA) in use.

The aim of this work is the investigation of major expansion and reshaping of MM-wave beams, which occur in defective-mode photonic bandgap resonators at the frequencies of resonant transmission. The effect is of particular importance for the accurate measurements of dielectric parameters of materials by quasi-optical resonator methods.

A basic form of quasi-optical resonator is a Fabry-Perot structure made of two dielectric layers placed at the distance L one from another [34]. Dielectric layers can be replaced by Bragg mirrors made of quarter-wavelength plates separated with air spaces. The Bragg mirror structures display much greater Q -factors and produce much greater increase of the resonant fields [1]. A single dielectric layer is also a resonator, though having a low Q -factor when using conventional dielectrics. By inserting a dielectric layer in a high- Q resonator, one produces a highly-sensitive system for the resonant spectroscopy of dielectric materials [35,36].

Record-breaking results obtained with quasi-optical resonators in MM- and sub-MM-wave bands are presented in [29–31] where Q -factors approaching one million have been achieved due to the use of large, dielectric-coated, extremely perfect metallic mirrors. Bragg structures in our research have smaller Q -factors as compared to the resonators in [29–31], though they are more suitable for measuring spatial profiles of MM-wave beams.

The expansion of beams increases spurious signals arising from the edge of material wafers due to the edge scattering and absorption, imperfections of rim processing, limitations in size and design of entire assembly. The research demonstrates beam expansion in a few kinds of typical structures. It shows that negative effects could be reduced by avoiding longitudinal higher-order resonances, increasing the size of wafers, improving their alignment, and reducing other irregularities in the system.

2. Multilayer structures

Reshaping of MM-wave beams transmitted through highly-resonant multilayer structures is investigated with both numerical simulation and experimental testing of spatial profiles of beams propagated through structures that should reveal essential features of this phenomenon.

A general view of structures is shown in Fig. 1. The structures are made as multilayer stacks of fused quartz wafers of thickness $q = 0.498$ mm interlaced with air spaces a and c as shown in Fig. 2(a). Each structure is designed as an open resonator of MM waves that consists of two Bragg mirrors separated by a resonant section. The structures are designated as $K(aq)-c-3q-c-K(qa)$ where q , a and c signify wafers and air spaces, respectively, K is the number of aq pairs in a Bragg mirror, and $3q$ is a stack of three wafers having the resonant thickness at $f = 102.9$ GHz (free-space wavelength $\lambda = 2.912$ mm) when the dielectric constant of wafers is $\varepsilon = 3.80$ (wavelength in fused quartz is $\lambda_q = \lambda/\sqrt{\varepsilon} = 3q = 1.494$ mm) [32,33].



Fig. 1. Multilayer quartz structures in (a) brass and (b) plastic frames.

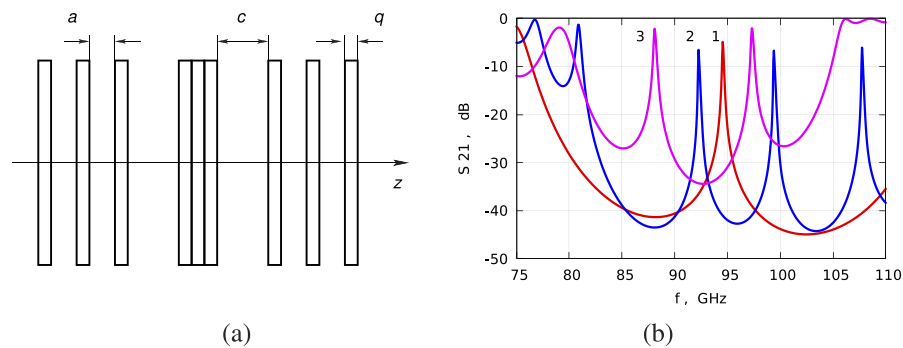


Fig. 2. (a) Schematic of a resonant structure. (b) Simulated transmission spectra of structures #1, #2, and #3 excited by a linearly polarized Gaussian beam (curves 1 to 3, respectively).

We consider three kinds of structures. Structures #1 and #2 are specified as $5(aq)-c-3q-c-5(qa)$ where $a = 0.508$ mm and c is either $c = 1.016$ mm (structure #1) or $c = 6.00$ mm (structure #2). Structure #3 is of the kind $4(aq)-c-3q-c-4(qa)$ where $a = 2.25$ mm and $c = 3.00$ mm. Structures #1 and #2 are mounted in brass frames of clear aperture diameter $D_C = 66$ mm, Fig. 1(a), whereas structure #3 is fixed in open plastic frames, Fig. 1(b), for minimizing the aperture effects (the wafer diameter is $D_q = 75$ mm). In structure #3, the aperture distance between the tips of plastic strips holding the wafers along the horizontal axis is $D_1 = 67$ mm whereas distance between the inner corners of frames along the axis at $\varphi = 22.5$ deg is $D_2 = 136$ mm.

MM-wave transmission spectra simulated for structures #1, #2, and #3 in the frequency band of $f = 75 - 110$ GHz are shown in Fig. 2(b). The spectra reveal resonant transmission peaks in the propagation bandgap of structures. Here, at the given wafers, parameter a controls the bandgap and c defines the number and location of peaks. In an ideal structure, $a = q\sqrt{\epsilon} = m\lambda/4$ (m is an odd number, $m = 1$ is optimal) and the optical thickness of $c-3q-c$ block is $n\lambda/2$ (n is an integer). Major reshaping of beams occurs at the peaks of resonant transmission.

3. Incident beams

MM-wave measurements were made using a VNA quasi-optical bench facility at the Maynooth University Department of Experimental Physics (Ireland). The bench is shown schematically in Fig. 3(a). It consists of a source horn H , a lens L , a device under test T , and a probe P , which is scanning the beam along the horizontal (x), vertical (y), and two diagonal (xy) cuts in the transverse plane behind the device.

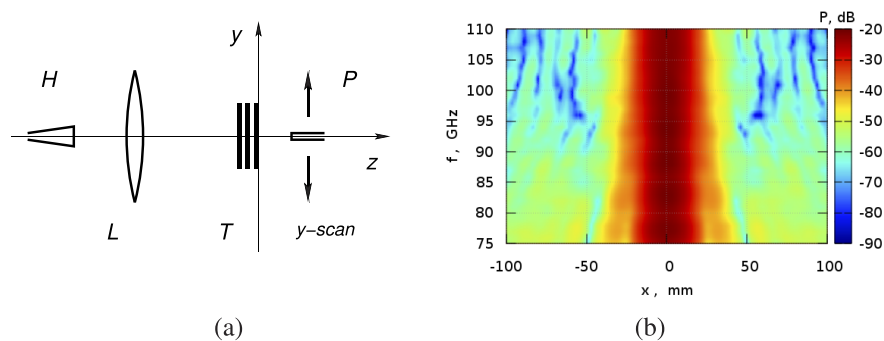


Fig. 3. (a) Schematic of quasi-optical bench. (b) Power P of the incident beam measured as a function of x and f in the x -cut ($y = 0$) in the focal plane of lens PTFE-2011 ($W_{E0} = 16$ mm).

The VNA (R&S ZVA24) is equipped with frequency extension heads (ZVA-Z110) for W-band operation. One head (h_1) is mounted as a single unit along with horn H and lens L and the other head (h_2) is carrying the probe. The lens is either one or another of custom-made Fresnel lenses marked as PTFE-2011 and PTFE-2013 in [37] (lenses L_1 and L_2 , respectively). The horn and lens create a nearly Gaussian beam of vertical polarization at the focal plane where the DUT is placed. Both the probe transverse movements and the axial positions z_n of the VNA head h_1 ($n = 1$) and the DUT unit ($n = 2$) are computer controlled using Zaber linear actuators. This allows us to perform standing wave filtering of recorded S_{21} signals as explained in [32].

The VNA system makes the records of beam power profile $P(x, y, z_n, f)$ as detected by the probe of rectangular aperture, which is sensitive to vertical component of electric field of incoming wave. As an example, Fig. 3(b) shows the power P of the incident beam as a function of x and f at $y = 0$ when measured in the focal plane of lens PTFE-2011.

Figure 4(a) shows radial cuts of measured (1, 3) and Gaussian fitted (2, 4) wave beams in the focal plane of lenses L_1 (1, 2) and L_2 (3, 4) at $f = 95$ GHz. Circular Gaussian fits are employed here and used later as the source beams in simulations. The radial cuts are centered at the beam axes defined by Gaussian fits, which in the measurement frame are about $x_{c0} = 0.5$ mm and $y_{c0} = 2.0$ mm. The Gaussian fits are found by choosing the fitting area radius R_F close to the beam radius W_{E0} defined by the electric field distribution $E(r) = E_0 \exp(-r^2/W_{E0}^2)$. This provides the best fitting of central part of each beam, with relevant values accepted as $R_F = W_{E0} = 16$ mm and 22 mm for lenses L_1 and L_2 , respectively.

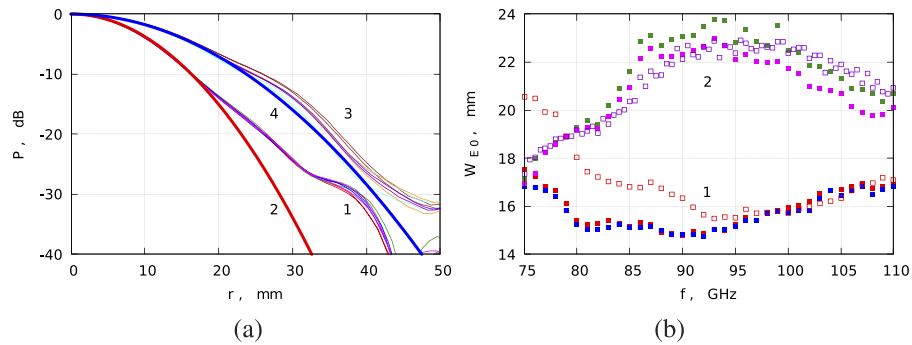


Fig. 4. (a) Radial cuts of measured (1, 3) and Gaussian fitted (2, 4) beams in the focal plane of lenses PTFE-2011 (1, 2) and PTFE-2013 (3, 4) at $f = 95$ GHz. (b) Radius $W_{E0}(f)$ of beams in different settings with lenses PTFE-2011 (1) and PTFE-2013 (2).

Figure 4(b) shows the frequency dependence of W_{E0} found at the precise position ($z = 0$) or slightly behind ($z = 46$ mm) the focal plane of lenses L_1 and L_2 (filled and empty points, respectively). In the band of $f = 85 - 105$ GHz, W_{E0} is nearly constant (within about ± 1 mm) at these positions and remains so regardless the insertion or removal of plastic holder of aperture diameter $D_H = 70$ mm, which is used for mounting structures assembled in various frames.

4. Computer simulations

Simulations of MM-wave beams utilize transmission matrix technique, which is extended for the beam propagation cases through the use of spatial Fourier transforms of beams and propagation of partial plane waves [32,33]. In the case of infinite aperture size, the technique provides an exact solution to the beam propagation problem when the incident beam is an exact solution to Maxwell's equations and the Fourier transform is exact. A beam of any profile specified by tangential field components at the entrance surface can be presented as an exact solution by restoring its correct vector structure as explained in [38] and implemented in our work.

Simulations of narrow beams ($W_{E0} = 16$ mm) passed through a dielectric slab ($3q$ stack at $f = 75 - 110$ GHz) or a simple Fabry-Perot resonator (q - c - q structure with quality factor $Q < 10$ at $c \leq 6$ mm) show minor width variations (below 1% for resonators and far less for slabs) that can be neglected. Multilayer assemblies like structures #1 to #3 defined above, on the contrary, reveal variations of beam width that can be significant at the resonant conditions.

Figure 5 shows the resonant peaks of transmission spectra as measured (points) and simulated (curves) for structures #1, #2, and #3. Simulations employ the Gaussian source beams produced with lenses L_2 (structure #1, $W_{E0} = 22$ mm) and L_1 (structures #2 and #3, $W_{E0} = 16$ mm).

The measured resonant frequencies are found to be $f_{1m} = 94.40$, $f_{2am} = 92.12$, $f_{2bm} = 99.47$ and $f_{3m} = 97.45$ GHz for the peaks 1, 2a, 2b, and 3, whereas simulated values are $f_{1s} = 94.54$, $f_{2as} = 92.25$, $f_{2bs} = 99.38$ and $f_{3s} = 97.32$ GHz, respectively. Q -factors for simulated peaks are $Q_{1s} = 839$, $Q_{2as} = 757$, $Q_{2bs} = 846$ and $Q_{3s} = 430$.

Figure 6(a) presents radial cuts of simulated beams at the exit plane of structure #2 in the vicinity of transmission peak 2b. Curves 1 to 6 are computed at frequencies $f = 99.2$ to 100.2 GHz with increments of 0.2 GHz. Power profiles $P(r)$ are normalized to $P(0) = 1$ at each frequency. Curve 7 shows the incident Gaussian beam of lens L_1 with $W_{E0} = 16$ mm. Radial cuts of beams simulated for structure #2 at peak 2a and for structures #1 and #3 at peaks 1 and 3, respectively, have a similar look.

Simulations show major expansion of beams transmitted through resonant multilayer structures at the frequencies of peak transmission, which are characterized by large values of quality factor

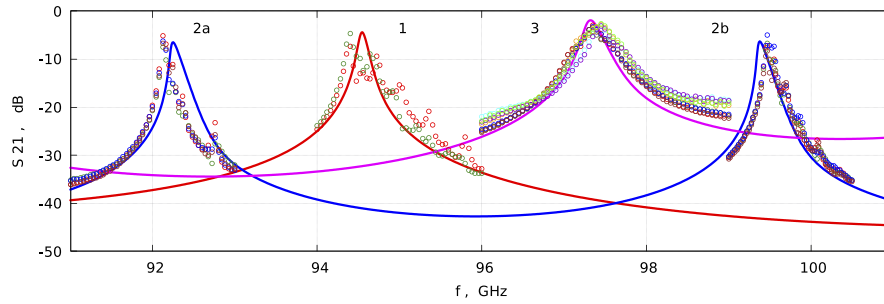


Fig. 5. Resonant peaks 1, 2a, 2b and 3 of measured (points) and simulated (curves) transmission spectra of structures #1, #2, and #3, respectively.

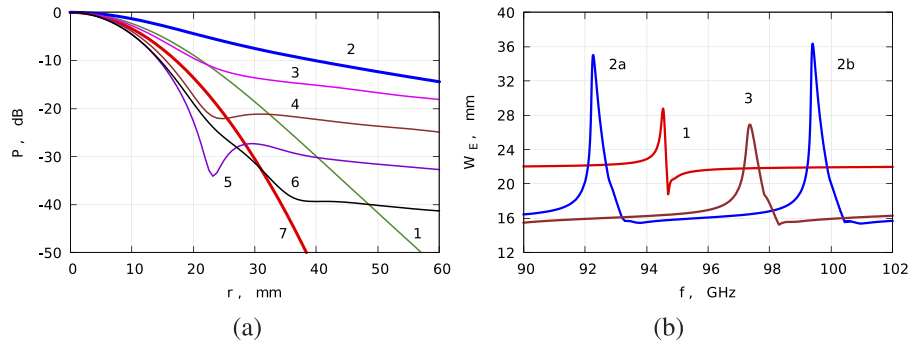


Fig. 6. (a) Radial cuts of beams simulated at the exit plane of structure #2 at some frequencies around peak 2b (curve 2, $f = 99.4$ GHz) using the source beam L_1 (curve 7, $W_{E0} = 16$ mm). (b) Radius W_E of simulated transmission beams for structures #1, #2, and #3 with resonant peaks 1, 2a, 2b, and 3, respectively.

Q . The beam radius W_E in each case grows rapidly, in a resonant manner, to reach a maximum at the resonant frequency, then, with increasing the frequency, drops slightly below the incident beam radius W_{E0} and gradually returns to W_{E0} at the frequencies away from the resonance.

All the transmitted beams preserve axial symmetry and vertical polarization imposed by the source beams. Gaussian fitting of simulated beams ($R_F = 30$ mm) reveals the frequency dependence of beam radius $W_E(f)$ for each structure as shown in Fig. 6(b). Reflected beams also show variations in width, which are, generally, opposite in sign to variations of transmitted beams, though they are less accessible for experimental investigation at normal incidence.

5. Experimental results

Experimental results for the beams transmitted through structures #1, #2 and #3 are presented in Figs. 7–11. Power profiles are measured in the plane $z = 46$ mm behind the exit aperture of each structure counting from the outer surface of external frame of assembly while the structure is centered at the focal plane of incident beam.

Figure 7 shows transmission beam axis coordinates x_c and y_c and the effective radius W_E found as the parameters of a circular Gaussian fit for each of the beams of structures #1, #2, and #3. The fitting area radius $R_F = 30$ mm is chosen to be close to the aperture radius $R_C = 33$ mm, being also close to the W_E values obtained. The results confirm resonant expansion of beams at the transmission peaks, showing approximate similarity of curves $W_E(f)$ in Figs. 7(b) and 6(b). They also show instability of beam width and axis position at the resonant frequencies.

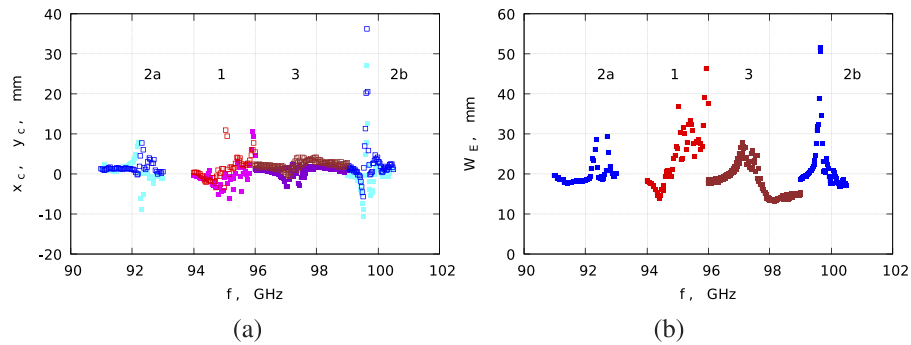


Fig. 7. (a) Transmission beam axis coordinates x_c and y_c (filled and empty points, respectively) and (b) beam radius W_E as found by Gaussian fitting of measured power profiles of structures #1, #2, and #3 with resonant peaks 1, 2a, 2b, and 3, respectively.

Figure 8 shows the beam power P as a function of coordinate x and frequency f at the resonant peak 2b of structure #2 presented for (a) simulated and (b) measured transmission beams. The structure displays the greatest beam expansion and instability of beam shape and position at resonant transmission. The measurements show significant distortion of transmitted beam at the frequencies above the frequency of resonant transmission $f_{2b_m} = 99.47$ GHz.

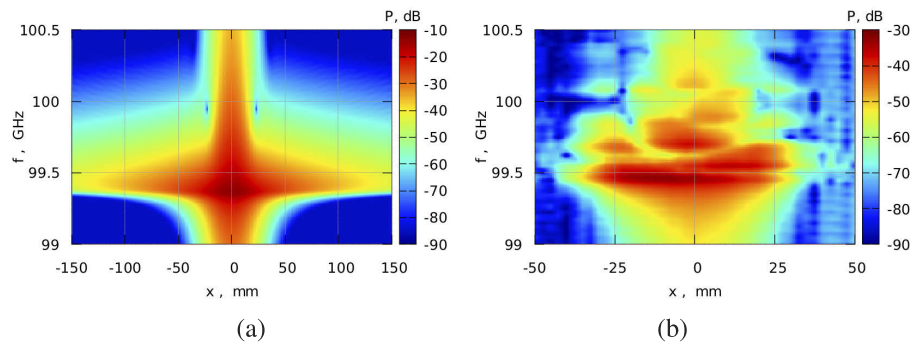


Fig. 8. (a) Simulated and (b) measured power P of transmitted beam behind structure #2, peak 2b, presented as a function of x and f .

Structure #2 is specified by large air spaces in its resonant section, which has total optical thickness $t = 5\lambda$ at $f \approx 100$ GHz. This helps in excitation of higher-order quasi-optical modes at the resonances. The excitation of higher-order modes in high- Q structures produces major reshaping of transmitted beams when the frequency exceeds the minimal resonant frequency of plane wave propagation.

Gaussian beams transmitted through structures of unlimited aperture acquire specific shapes that have the inner parts with Gaussian profile of increased, at the resonance, radius W_E and the outer parts with extended exponential decay, Fig. 6(a). Further reshaping of beams is induced by the limited aperture and irregularities of real structures.

Major distortion of transmitted beam is observed in Fig. 9. It shows power P as a function of x and f in horizontal and vertical cuts of beam transmitted through structure #1, peak 1, which is excited by the source beam of lens L_2 ($W_{E0} = 22$ mm). According to simulations, the maximum radius of transmitted beam, if not limited by the aperture, is $W_E = 27.3$ mm. In this case, the power at the aperture rim computed with respect to on-axis power is $P_{ri} = -20$ dB and $P_{rt} = -19$ dB for the incident and transmitted beams, respectively.

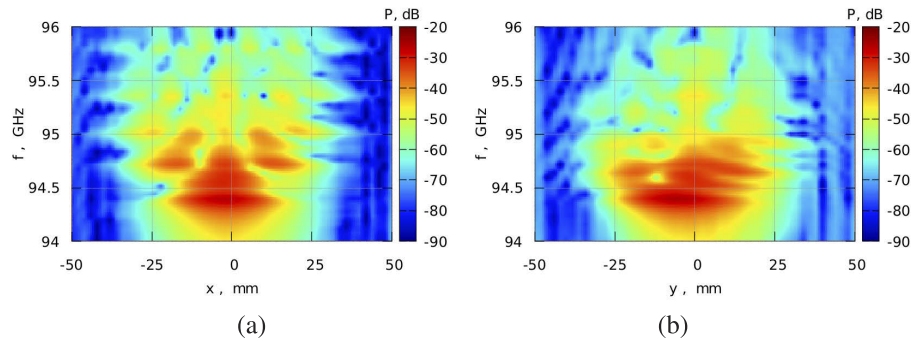


Fig. 9. Beam power P as a function of scan coordinate and frequency as measured behind structure #1, peak 1, in (a) horizontal ($y = 0$) and (b) vertical ($x = 0$) cut.

In the experiment, the rim power of transmitted beam exceeds $P_{rt} = -15$ dB and even $P_{rt} = -10$ dB at peak frequencies between $f = 94.50$ and 94.80 GHz. The power is quite noticeable and may produce the aperture rim effects responsible for specific pattern of beam distortion in Fig. 9(a). A less regular pattern in Fig. 9(b) may arise due to a minor tilt of structure #1 that was eliminated in other experiments.

In relative terms, the resonant beam expansion is greater for narrow beams and high- Q structures. In structure #2, peak 2b, the radius of simulated beam in the case of lens L_1 ($W_{E0} \approx 5\lambda$) increases 2.3 times to $W_{E1} = 36.4$ mm, whereas in the case of lens L_2 ($W_{E0} \approx 7\lambda$) it grows only 1.6 times to $W_E = 35.7$ mm (in this case, $Q = 1215$).

Large values of W_E and exponential rather than Gaussian beam "tail" lead to the resonant increase of the aperture rim power. For this reason, in measurements of dielectric losses with high- Q resonator methods [29–33], rim effects could be much greater than initially expected.

Significant distortion of beams leads to degradation of perfect shape of resonant peaks in the transmission spectra $S_{21}(f)$ of structures at the frequencies just above the peak values, see Fig. 5. Each of S_{21} points is computed here as a scalar product of structure transmission beam and lens-and-horn receiver beam assuming the horn-to-horn system in [32,33]. Unlike the spectra in Fig. 5, S_{21} curves in [32,33] had been measured directly. Neither of curves in [32,33] show degradation of transmission peaks. This is because the structures have low Q -factors, $Q \sim 300$. Yet, structures with higher Q -factors do show degradation of peaks in direct measurements. The resonant beam distortion provides the explanation of the effect whereas degradation of peaks serves as an indication of beam distortion.

For reducing the aperture effects, we made an "open" structure #3 where quartz wafers are suspended in air by means of plastic frames, which hold the wafers with tips of narrow radial strips and use no metallic elements.

Figure 10 shows power profiles of beams measured in different cuts behind the structure #3 at the transmission peak 3 when the x axis is (a) horizontal and (b) tilted at $\varphi = 22.5$ deg about z axis. Filled and empty points present power profiles at the peak frequency $f_{3m} = 97.45$ GHz where transmitted beam is most expanded and at the higher frequency $f = 99.00$ GHz where the beam is close to the incident one, respectively (each profile $P(r)$ is normalized to $P_{\max} = 1$).

Power profiles near the resonant frequency are unstable in shape when compared between different cuts and adjacent frequency points. This property is common for all kinds of structures and resonant frequencies. To make data more representative, Fig. 10 shows the mean power profiles of beams, solid curves 1 to 3, evaluated for two transmitted and one incident beam, respectively. Each curve is computed as the arithmetic average over four cuts and three adjacent frequency points centered at the representative frequency (e.g., 97.40, 97.45, and 97.50 GHz for curve 1) when taking power in relative units and, after the averaging, normalizing it to $P_{\max} = 1$.

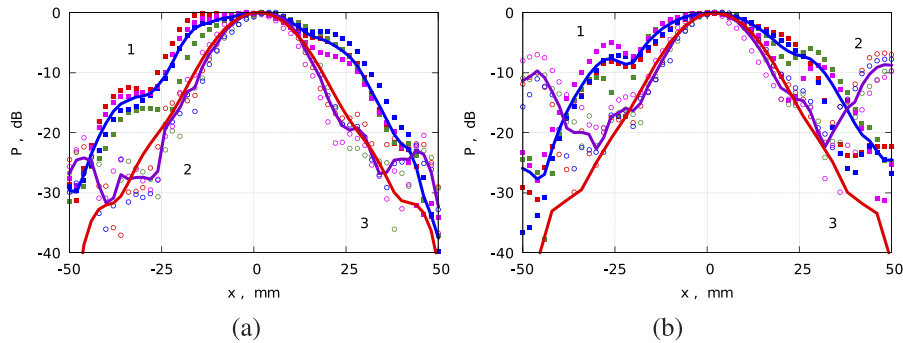


Fig. 10. Profiles of beam power P measured behind structure #3, peak 3, when the x axis is (a) horizontal and (b) tilted at $\varphi = 22.5$ deg about z axis (notations are explained in the text).

Curves 1 and 2 correspond to transmitted beams at $f = 97.45$ and 99.00 GHz, respectively, and curve 3 shows the incident beam at $f = 97.45$ GHz.

Figure 11 shows the beam power P as a function of x and f behind structure #3 when the x axis is (a) horizontal and (b) tilted at $\varphi = 22.5$ deg about z axis. Both the Figs. 10–11 demonstrate the expansion, distortion, and asymmetry of transmitted beams at the resonant frequency. At the same time, they show that, with "open" plastic frames, transmitted beams remain better shaped and more expanded (despite nearly twice smaller Q -factor) when compared to the beams of other structures, thus, producing the measurement results more consistent with simulations.

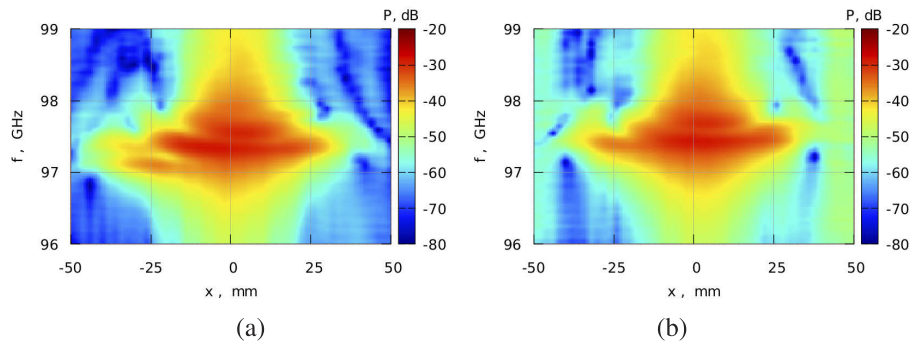


Fig. 11. Beam power P measured as a function of x and f behind structure #3, peak 3, when the x axis is (a) horizontal and (b) tilted at $\varphi = 22.5$ deg about z axis.

6. Conclusions

We observed major reshaping and expansion of MM-wave beams transmitted through resonant multilayer structures. Both the experiments and simulations reveal that reshaping and expansion of beams become significant when Q -factors of structures achieve sufficiently large values.

In structures designed as Bragg resonators with Q -factor ~ 800 in the MM-wave band ($f = 75 - 110$ GHz), the effective radius W_E of transmitted beam increases at the resonant frequencies 2 to 3 times as compared to the incident beam radius $W_{E0} \approx 16 - 22$ mm, which is similar to approximate estimates [27] at oblique incidence. The resonant beam expansion is accompanied by distortion of beam profile, which is characterized by extreme variations of beam width, overall shape, and position of beam center.

The expansion and reshaping of beams emerges due to efficient excitation of intrinsic quasi-optical modes of complex spatial profiles at resonant frequencies. The beams also become very sensitive to irregularities of multilayer structures and imperfections of alignment of quasi-optical bench components.

The beam expansion belongs to the same group of effects as the Goos-Hänchen and Imbert-Fedorov effects [9–11], which appear in multilayer systems [12–14], in structures with additional resonant enhancements [19–26] and, particularly, in defect-mode photonic crystals [27,28]. The effect is more noticeable for narrow beams, whose radius is just a few radiation wavelength. It also imposes high precision requirements on multilayer structures for making high- Q resonators. Therefore, the effect may better be observed in the MM-wave band rather than in optics.

The beam expansion leads to a resonant jump of the aperture rim effects. For example, in structure #3, peak 3, Fig. 10, the beam power at the aperture rim measured with respect to on-axis power may grow from -30 dB to -15 dB at the resonant frequency. This increases the relative contribution of rim power losses at the resonant conditions.

The effect is important for the resonant methods of MM-wave and THz spectroscopy of low-loss dielectric materials [29–32]. It is a parasitic effect that has to be avoided. For this, much smaller beam width as compared to wafer diameter has to be used than conventionally required. The angular alignment has also to be enhanced because of similar angular effects.

In practice, since the resonant rim effects are hard to predict, dielectric parameters should be recovered by using a series of measurements with different incident beams. Then, a critical beam width should be found so that the parameters obtained with narrower beams to remain constant, thus, providing the results insensitive to the aperture rim.

Major distortions of beams would also produce systematic errors. The distortions are quite irregular and emerge due to poorly defined shape of intrinsic modes in the transverse directions. This is a reason for ill-conditioned character of problems at resonances, which is a source of instabilities in both experiments and simulations. These instabilities make exact simulations quite uninformative for comparison with experiment and, at the same time, indispensable for obtaining the information on field profiles at resonances.

In summary, transmission of narrow beams through high-quality multilayer structures produces major reshaping and spatial expansion of beams at the frequencies of resonant transmission. Distortion of beams leads to degradation of perfect shape of resonant peaks in the transmission frequency spectra that, in due turn, serves as an indication of beam reshaping. Major distortion and expansion of beams in ultra-high- Q structures has to be taken into account in applications such as the resonant spectroscopy of low-loss dielectric materials, measurements of layer thickness in multilayer assemblies, and similar problems.

Acknowledgments

The VNA laboratory at Maynooth University Department of Experimental Physics was originally funded by Science Foundation Ireland. The authors are grateful to D. Watson, Maynooth University, Maynooth, Ireland, and I. Yeniay, Ayteknoloji Ltd, Ankara, Turkey, for high-precision fabrication of components for MM-wave experiments.

Disclosures

The authors declare no conflicts of interest.

References

1. H. A. Macleod, “*Thin-Film Optical Filters*,” 3rd Ed., (IOP, 2001).
2. T. Ooya, M. Tateiba, and O. Fukumitsu, “Transmission and reflection of a Gaussian beam at normal incidence on a dielectric slab,” *J. Opt. Soc. Am.* **65**(5), 537–541 (1975).
3. M. Tanaka, K. Tanaka, and O. Fukumitsu, “Transmission and reflection of a Gaussian beam at oblique incidence on a dielectric slab,” *J. Opt. Soc. Am.* **67**(6), 819–825 (1977).

4. R. P. Riesz and R. Simon, "Reflection of a Gaussian beam from a dielectric slab," *J. Opt. Soc. Am. A* **2**(11), 1809–1817 (1985).
5. J. J. Cowan and B. Anicin, "Longitudinal and transverse displacements of a bounded microwave beam at total internal reflection," *J. Opt. Soc. Am.* **67**(10), 1307–1314 (1977).
6. Q. Li and R. J. Vernon, "Theoretical and experimental investigation of Gaussian beam transmission and reflection by a dielectric slab at 110 GHz," *IEEE Trans. Antennas Propag.* **54**(11), 3449–3457 (2006).
7. D. Müller, D. Tharanga, A. A. Stahlhofen, and G. Nimtz, "Nonspecular shifts of microwaves in partial reflection," *Europhys. Lett.* **73**(4), 526–532 (2006).
8. Q. Li, B. Zhang, and J. Shen, "Goos-Hänchen shifts of reflected terahertz wave on a COC-air interface," *Opt. Express* **21**(5), 6480–6487 (2013).
9. K. Y. Bliokh and A. Aiello, "Goos-Hänchen and Imbert-Fedorov beam shifts: An overview," *J. Opt.* **15**(1), 014001 (2013).
10. A. Aiello, M. Merano, and J. P. Woerdman, "Duality between spatial and angular shift in optical reflection," *Phys. Rev. A* **80**(6), 061801 (2009).
11. M. Merano, A. Aiello, M. P. van Exter, and J. P. Woerdman, "Observing angular deviations in the specular reflection of a light beam," *Nat. Photonics* **3**(6), 337–340 (2009).
12. T. Tamir and H. L. Bertoni, "Lateral displacement of optical beams at multilayered and periodic structures," *J. Opt. Soc. Am.* **61**(10), 1397–1413 (1971).
13. T. Tamir, "Nonspecular phenomena in beam fields reflected by multilayered media," *J. Opt. Soc. Am. A* **3**(4), 558–565 (1986).
14. G. D. Landry and T. A. Maldonado, "Gaussian beam transmission and reflection from a general anisotropic multilayer structure," *Appl. Opt.* **35**(30), 5870 (1996).
15. M. Merano, "Optical beam shifts in graphene and single-layer boron-nitride," *Opt. Lett.* **41**(24), 5780–5783 (2016).
16. S. Chen, C. Mi, L. Cai, M. Liu, H. Luo, and S. Wen, "Observation of the Goos-Hänchen shift in graphene via weak measurements," *Appl. Phys. Lett.* **110**(3), 031105 (2017).
17. X. Yin and L. Hesselink, "Goos-Hänchen shift surface plasmon resonance sensor," *Appl. Phys. Lett.* **89**(26), 261108 (2006).
18. L. Salasnich, "Enhancement of four reflection shifts by a three-layer surface-plasmon resonance," *Phys. Rev. A* **86**(5), 055801 (2012).
19. Y. Wan, Z. Zheng, W. Kong, X. Zhao, Y. Liu, Y. Bian, and J. Liu, "Nearly three orders of magnitude enhancement of Goos-Hänchen shift by exciting Bloch surface wave," *Opt. Express* **20**(8), 8998–9003 (2012).
20. I. V. Soboleva, V. V. Moskalenko, and A. A. Fedyanin, "Giant Goos-Hänchen effect and Fano resonance at photonic crystal surfaces," *Phys. Rev. Lett.* **108**(12), 123901 (2012).
21. P. Hou, Y. Chen, X. Chen, J. Shi, and Q. Wang, "Giant bistable shifts for one-dimensional nonlinear photonic crystals," *Phys. Rev. A* **75**(4), 045802 (2007).
22. R.-R. Wei, X. Chen, J.-W. Tao, and C.-F. Li, "Giant and negative bistable shifts for one-dimensional photonic crystal containing a nonlinear metamaterial defect," *Phys. Lett. A* **372**(45), 6797–6800 (2008).
23. P. R. Berman, "Goos-Hänchen shift in negatively refractive media," *Phys. Rev. E* **66**(6), 067603 (2002).
24. I. V. Shadrivov, A. A. Zharov, and Y. S. Kivshar, "Giant Goos-Hänchen effect at the reflection from left-handed metamaterials," *Appl. Phys. Lett.* **83**(13), 2713–2715 (2003).
25. W.-W. Deng, S.-P. Wu, and G.-X. Li, "Enhancement of the Goos-Hänchen shift by electromagnetically induced transparency with amplification," *Opt. Commun.* **285**(10–11), 2668–2674 (2012).
26. X.-J. Zhang, H.-H. Wang, C.-L. Wang, Y. Xu, Z.-P. Liang, C.-B. Fan, C.-Z. Liu, and J.-Y. Gao, "Goos-Hänchen shift of the reflected beam in a standing-wave coupled electromagnetically induced transparency system," *J. Opt. Soc. Am. B* **32**(11), 2281–2287 (2015).
27. L.-G. Wang and S.-Y. Zhu, "Giant lateral shift of a light beam at the defect mode in one-dimensional photonic crystals," *Opt. Lett.* **31**(1), 101–103 (2006).
28. D. Zhao, F. Liu, P. Meng, J. Wen, S. Xu, Z. Li, and D. Zhong, "Reflection enhancement and giant lateral shift in defective photonic crystals with graphene," *Appl. Sci.* **9**(10), 2141 (2019).
29. A. F. Krupnov, V. N. Markov, G. Y. Golubiatnikov, I. I. Leonov, Y. N. Konoplev, and V. V. Parshin, "Ultra-low absorption measurement in dielectrics in millimeter- and submillimeter-wave range," *IEEE Trans. Microwave Theory Tech.* **47**(3), 284–289 (1999).
30. A. F. Krupnov, M. Y. Tretyakov, S. P. Belov, G. Y. Golubiatnikov, V. V. Parshin, M. A. Koshelev, D. S. Makarov, and E. A. Serov, "Accurate broadband rotational BWO-based spectroscopy," *J. Mol. Spectrosc.* **280**, 110–118 (2012).
31. V. V. Parshin, M. Y. Tretyakov, M. A. Koshelev, and E. A. Serov, "Modern resonator spectroscopy at submillimeter wavelengths," *IEEE Sens. J.* **13**(1), 18–23 (2013).
32. V. B. Yurchenko, M. Ciydem, M. L. Gradziel, and L. V. Yurchenko, "MM-wave dielectric parameters of magnesium fluoride glass wafers," *Prog. Electromagn. Res. M* **62**, 89–98 (2017).
33. V. B. Yurchenko, M. Ciydem, M. L. Gradziel, J. A. Murphy, and A. Altintas, "Light-controlled photonics-based mm-wave beam switch," *Opt. Express* **24**(15), 16471–16478 (2016).
34. H. Kogelnik and T. Li, "Laser beams and resonators," *Appl. Opt.* **5**(10), 1550–1567 (1966).

35. J. Baker-Jarvis, M. D. Janezic, B. F. Riddle, R. T. Johnk, P. Kabos, C. L. Holloway, R. G. Geyer, and C. A. Grosvenor, “*Measuring the Permittivity and Permeability of Lossy Materials: Solids, Liquids, Metals, Building Materials, and Negative-Index Materials*,” (NIST, 2005).
36. V. N. Egorov, “Resonance methods for microwave studies of dielectrics (review),” *Instrum. Exp. Tech.* **50**(2), 143–175 (2007).
37. V. B. Yurchenko, M. Ciydem, M. Gradziel, J. A. Murphy, and A. Altintas, “Double-sided split-step mm-wave Fresnel lenses: Fabrication and focal field measurements,” *J. Europ. Opt. Soc. Rap. Public.* **9**, 14007 (2014).
38. G. Zhou, X. Chu, and J. Zheng, “Analytical structure of an apertured vector Gaussian beam in the far field,” *Opt. Commun.* **281**(8), 1929–1934 (2008).